

# PARTICLE SWARM OPTIMIZATION OF SOLAR CENTRAL RECEIVER SYSTEMS FROM A MONTE CARLO DIRECT MODEL

Olivier Farges, Jean-Jacques Bézian, Mouna El-Hafi, Olivier Fudym, Hélène Bru

#### ▶ To cite this version:

Olivier Farges, Jean-Jacques Bézian, Mouna El-Hafi, Olivier Fudym, Hélène Bru. PARTICLE SWARM OPTIMIZATION OF SOLAR CENTRAL RECEIVER SYSTEMS FROM A MONTE CARLO DIRECT MODEL. IPDO 2013: 4th Inverse problems, design and optimization symposium, Jun 2013, Albi, France. hal-01163826

### HAL Id: hal-01163826 https://imt-mines-albi.hal.science/hal-01163826

Submitted on 15 Jun 2015

**HAL** is a multi-disciplinary open access archive for the deposit and dissemination of scientific research documents, whether they are published or not. The documents may come from teaching and research institutions in France or abroad, or from public or private research centers.

L'archive ouverte pluridisciplinaire **HAL**, est destinée au dépôt et à la diffusion de documents scientifiques de niveau recherche, publiés ou non, émanant des établissements d'enseignement et de recherche français ou étrangers, des laboratoires publics ou privés.

## PARTICLE SWARM OPTIMIZATION OF SOLAR CENTRAL RECEIVER SYSTEMS FROM A MONTE CARLO DIRECT MODEL

Olivier Farges<sup>a,b</sup>, Jean-Jacques Bézian<sup>a</sup>, Mouna El Hafi<sup>a</sup>, Olivier Fudym<sup>a</sup>, and Hélène Bru<sup>b</sup>

<sup>a</sup>Centre RAPSODEE, UMR CNRS 5302, École des Mines d'Albi-Carmaux, Université de Toulouse, 81013 Albi Cedex 09, France, olivier.farges@mines-albi.fr, jean-jacques.bezian@mines-albi.fr, mouna.elhafi@mines-albi.fr, olivier.fudym@mines-albi.fr

<sup>b</sup>Total New Energies, R&D - Concentrated Solar Technologies, Tour Michelet ,Paris La Défense, France, helene.bru@total.com

#### **Abstract**

Considering the investment needed to build a solar concentrating facility, the performance of such an installation has to be maximized. This is the reason why the preliminary design step is one of the most important stage of the project process. This paper presents an optimization approach coupling a Particle Swarm Optimization algorithm with a Monte Carlo algorithm applied to the design of Central Receiver Solar systems. After the validation of the direct model from experimental data, several PSO algorithms are tested to pick out efficient parameters.

#### **Nomenclature**

Roman	symbols		mal $n_1$		
B	Blocking performance in %	$N_m$	Number of mirrors constituting heliostat		
CRS	Central Receiver System	$p_i^k$	Particle $i$ best position after $k$ iterations		
$c_1$	Attraction parameter for individual behav-	PSO	Particle Swarm Optimizer		
	ior of the particle	$r_1$	Random number $r_1 \sim U(0,1)$		
$c_2$	Attraction parameter for social behavior of	$r_2$	Random number $r_2 \sim U(0,1)$		
	the particle	$r(x^*)$	Normalized cost reduction		
DNI	Direct normal irradiance in $W \cdot m^{-2}$	Sh	Shadowing performance in %		
$d(r(x^*))$	)) Distance to the maximum obtained cost	Sp	Spillage performance in %		
	reduction	$s_c$	Threshold for the number of successes dur-		
E	Yearly average energy in kWh		ing GCPSO run		
f	Target function	$S_m$	Size of mirrors constituting heliostats in m		
$f_c$	Threshold for the number of failures during	$S_{\mathcal{H}^+}$	Area of mirror in $m^2$		
	GCPSO run	${\mathcal T}$	Target (the exponent + indicate the active		
$g^k$	Global best position of the swarm after $k$		side)		
	iterations	t	Time in s		
GCPS	O Guaranteed Convergence Particle Swarm	TMY	Typical Meteorological Year		
	Optimizer	$v_i^k$	Current velocity of the $i$ particle at the $k$ it-		
${\cal H}$	Heliostats surface (the exponent + indicate		eration		
	the active side)	$\hat{w}$	Monte Carlo weight		
H	The Heaviside step function	w	Inertia weight		
$H_t$	Height of the CRS Tower in m	$w_{max}$	Maximum value of the weight inertia		
$k_{max}$	Number of iterations performed during	$w_{min}$	Minimum value of the weight inertia		
	PSO run	$x_i^k$	Current position of the $i$ particle at the $k$ it-		
$n_1$	Ideal normal at $x_1$	-	eration		
$n_h$	Effective normal at $x_1$ around the ideal nor-	$x^b$	Best particle of the reference case $a$		

$x^*$	Best particle for each test case	$\Omega_S$	Solar cone in sr		
$\hat{x}$	Best particle among all test cases	$\omega_1$	Direction after reflection in rad		
$y_j$	Point in the geometry	$\omega_S$	Direction inside the solar cone in rad		
Greek symbols		$ ho^k$	Scaling factor applied in GCPSO		
$\eta$	Hour in h: min: s	au	Index of the swarm best particle		
$\gamma$	Day of the year				

#### Introduction

A Central Receiver System (CRS) is a complex set composed of several different subsystems including heliostat field, tower, receiver, heat transport system, power conversion system, plant control, optionally a thermal energy storage, etc. To generate heat further used to produce electricity, synthetize solar fuels or supply an industrial process, the solar radiation is first reflected and concentrated by an heliostat field onto a receiver located at the top of a tower. A large proportion of the cost of a CRS plant is devoted to the heliostat field ( $\sim 50\%$ ) according to [1]. In consequence, it's necessary to pay special attention to this item during the preliminary design step of any CRS. Since the 70's, several studies have been dedicated to the optimization of central receiver systems and most of them specifically on heliostat fields. Among the most recent developments, we can quote [2], [3], [4] and [5]. Each of these studies deal with a specific set of parameters (either those describing the layout of the heliostat field, or the heliostat geometrie and size, or the height of the tower...). Evaluation of performance is often based on optical efficiency estimation. This parameter agregates reflection efficiency, cosine efficiency, interception efficiency, blocking and shadowing efficiency and transmission efficiency. These efficiency values are usually obtained from simplified mathematical models or ray tracing simulations with the constraint accomplishing optimization step in a reasonable computational time.

#### 1. Model descrition

In this paper, we present a new approach using a direct model based on Monte Carlo methods that is further combined with a stochastic optimization algorithm. Achievement of an optimization task requires an efficient direct model related to the target function used during optimization process.

#### 1.1 Modeling the annual energy collected

In the present case, the direct model simulates a central receiver system. It estimates the annual performance of a CRS by evaluating the annual energy collected at the receiver and the optical efficiency. From a radiative point of view, the evaluated quantity is the solar energy E at the entrance of a receiver after concentration by the heliostat field. In order to evaluate E, the direct model has to track positions of the sun of a typical year cycle. Doing so, all the geometry is dynamic, *i.e.* heliostats are redirected according to sun position. The quantity of interest is linked to the solar radiation data for a chosen area, coming from Typical Meteorological Year (TMY) file. Being a function of the Direct Normal Irradiance (DNI), the annual energy's estimation requires a DNI value for each instant. This value is obtained from linear interpolation between consecutive TMY data which are sampled every hour.

#### 1.2 Monte Carlo algorithm

Monte Carlo method, due to its integral formulation, allows a better convergence of the algorithm. Several CSP algorithms are developed in accordance with this principle [6] (central receiver systems, Fresnel linear collectors, fluidized bed receiver, enclosed solar photobioreactor). An overview of the specific Monte Carlo algorithm, dealing with the sun's positions in the sky, is presented on Fig. 1. This algorithm samples some dates from a uniform distribution, then locations on the heliostat field where sun rays are first reflected, after which it follows rays behavior in the CRS, *ie* computes reflections until each ray hits the final receiver:

- (1) A position of the sun is uniformly sampled over the year with a day  $\gamma$  and an hour  $\eta$
- (2) A location  $y_1$  is uniformly sampled on the reflective surface of the whole heliostat field  $\mathcal{H}^+$  of surface  $S_{\mathcal{H}^+}$
- (3) A direction  $\omega_s$  is uniformly sampled within the solar cone  $\mathcal{C}$  of angular radius  $\Omega_s$ . In order to identify shadowing effects, the location  $y_0$  is defined as the first intersection with a solid surface of the ray starting at  $y_1$  in the direction  $\omega_s$ :
  - (a) If  $y_0$  belongs to heliostat surface  $\mathcal{H}$  or to the receiver  $\mathcal{T}$ , a shadowing effect appears and the algorithm restarts at (1) with Monte Carlo weight  $\hat{w}_{out} = 0$ ;
  - (b) If  $y_0$  doesn't exist, the reflected direction  $\omega_1$  is sampled so as to represent reflection and pointing imperfections. The location  $y_2$  defined as the first intersection of the ray starting at  $y_1$  in the direction  $\omega_1$  is checked:
    - (i) If  $y_2$  belongs to something else than the receiver  $\mathcal{T}$ , there is a blocking effect and the algorithm restarts at (1) with Monte Carlo weight  $\hat{w}_{out} = 0$ ;
    - (ii) If  $y_2$  doesn't exist, there is a spillage effect and the algorithm restarts at (1) with Monte Carlo weight  $\hat{w}_{out} = 0$ ;
    - (iii) If  $y_2$  belongs to the receiver  $\mathcal{T}$ , the algorithm restart at (1) with Monte Carlo weight  $\hat{w}_{in} = DNI \times (\boldsymbol{\omega_s} \cdot \boldsymbol{n_h}) \times S_{\mathcal{H}^+}$  where  $\boldsymbol{n_h}$  is the effective normal at  $y_1$  around the ideal normal vector  $\boldsymbol{n_1}$ ;

This algorithm is equivalent to the integral formulation presented in Eq. (1).

$$E = \int_{1}^{365} p_{\Gamma}(\gamma) d\gamma \int_{0A.M.}^{12P.M.} p_{H}(\eta) d\eta \int_{\mathcal{H}^{+}} p_{Y_{1}}(\boldsymbol{y_{1}}) d\boldsymbol{y} \int_{\Omega_{S}} p_{\Omega_{S}}(\boldsymbol{\omega_{S}}) d\boldsymbol{\omega_{S}} \times \left\{ H(\boldsymbol{y_{0}} \in (\mathcal{H} \cup \mathcal{T})) \hat{w}_{out} + H(\boldsymbol{y_{0}} \notin (\mathcal{H} \cup \mathcal{T}) \times \int_{D_{N_{h}}} p_{N_{h}}(\boldsymbol{n_{h}} | \boldsymbol{\omega_{S}}; p) d\boldsymbol{n_{h}} \left\{ H(\boldsymbol{y_{2}} \notin \mathcal{T}) \hat{w}_{out} + H(\boldsymbol{y_{2}} \in \mathcal{T}) \hat{w}_{in} \right\} \right\}$$

$$(1)$$

#### 1.3 A specific computing framework

The direct model is implemented in the numerical framework EDStaR. This tool yields the practical implementation of a Monte Carlo algorithm for the radiative heat transfer model, making use of an integral formulation, and takes in consideration zero-variance approaches and sensitivity estimation as presented by [7] and [8]. Taking advantage of advanced rendering techniques developed by the computer graphics community, it can manage complex geometries with the use of the numerical library PBRT (Physically Based Rendering Techniques) [9]. It benefits of all the modern possibilities of computing such as massive parallelization and acceleration of the ray tracing in a complex geometry. Many solar applications have already been simulated with this tool. EDStaR permits a very efficient implementation of the direct model. With this tool, updating the geometry is performed quickly and achieving a fast simulation process takes less than a minute for 50 000 realizations to simulate a CRS with 74 880m<sup>2</sup> of mirror on a linux computer with AMD Phenom II X6 1055T 2.8GHz and 12Go RAM.

#### 1.4 Model validation

In order to validate the direct model, we simulate an existing CRS. Due to its quality of world's first commercial concentrating solar power tower, the comparison is done with PS10 Solar Power Plant. This CRS, operating near Seville, in Spain, is composed of a 115m high tower and a solar field with 164 heliostats ( $120\mathrm{m}^2$  each) arranged in a radial staggered layout [10]. According to measurements, the annual thermal energy collected at the entrance of the receiver is roughly 117GWh. We simulate this CRS with the direct model and appropriate irradiance data and obtain an annual thermal energy evaluation of  $113.8\mathrm{GWh} \pm 0.3$ . We conclude that the model is accurate, taking into account the significant variation which can appear between typical meteorological year data and the real weather.

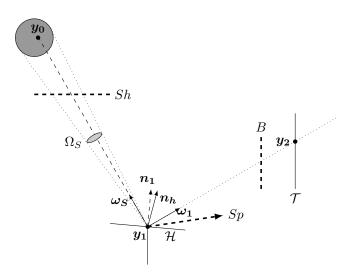


Fig. 1. Schematic representation of the ray tracing process on a Central Receiver System

#### 2. Optimization

The aim of this work is to build an optimization approach for the design Central Receiver Systems. We have to couple a direct model, presented in previous section with an optimization method.

#### 2.1 Target function and parameters

In our study, we define a target function accounting for the annual thermal energy at the entrance of the receiver using the direct model. We focus on parameters determining the layout of the heliostat field and the tower. The setting-up of heliostats is done accordingly to the MUEEN method [11]. This graphical method is a no-blocking radial staggered layout. The MUEEN method is based on an iterative algorithm which add an heliostat to the field until a regulatory limit is reached. In our case, the restriction concern the reflective surface. Once the limit is reached, the addition of heliostat is stopped. There are several ways to design an heliostat field with this method. We make the choice to release heliostats geometry: each heliostat is a set of square flat mirrors fixed on a curved structure. The design parameters are:

- The number of mirrors for each heliostat  $N_m$
- The size  $S_m$  of flat mirrors
- The height of the tower  $H_t$

Due to the several constraints to respect in a CRS design, some limitations exist. Free parameters are then restricted by lower and upper bounds. The aim of optimization is to maximize the target function dealing with these parameters. To identify the most adapted method, we have to investigate particularities of the target function. Derivatives to parameters that modify the domain of integration can hardly be obtained by Monte Carlo method as presented by [12]. As a consequence, gradient method can't be applied in this case. Another remarkable characteristic is the non-smooth target function due to MUEEN method. A small variation in the parameters can cause a radical change of the field geometry.

#### 3. Stochastic optimization with PSO

Among all existing optimization methods we make the choice to focus on stochastic algorithms and, more specifically on particle swarm optimization (PSO). It is proved in [13] that PSO is an efficient optimization method when dealing with non-smooth simulation-based optimization. A particle swarm optimization algorithm, as a zero order optimization method, doesn't need to have derivatives with respect to one of the free parameters. Furthermore, PSO is a stochastic method and then allow us to find the global optimum among all local optima. This well-known population-based optimization method was first introduce by [14]. According to this algorithm, each particle i of the swarm has, at iteration k, a position  $x_i^k$  in the search space, a velocity  $v_i^k$  and a personal best position  $p_i$ . This personal best position corresponds to the  $x_i$  maximizing the target function f. Furthermore, the algorithm considers g which is the global best position, i.e. among the particles of the swarm, the position of the one giving the highest target function. At iteration k+1, each particle position  $x_i^{k+1}$  is updated with its previous position  $x_i^k$  and its updated velocity  $v_i^{k+1}$ , as presented in Eqs. (2) and (3). The 2 numbers  $r_1$  and  $r_2$  are random numbers uniformly sampled in [0,1] and used to effect the stochastic nature of the algorithm. The weight inertia w is used to control the convergence behavior of the PSO. A dynamic inertia is also implemented: the value of inertia varies with the iteration k, decreasing linearly with k as presented in Eq. (4). The coefficients  $c_1$  and  $c_2$  control how far a particle will move in the search space in a single iteration.  $c_1$  leads the individual behavior of the particle whereas  $c_2$  leads its social behavior. In addition, a velocity clamping is set with a maximum velocity gain  $|v_{max}| = 4$ .

$$v_i^{k+1} = w \times v_i^k + c_1 \times r_1 \times (p_i - x_i^k) + c_2 \times r_2 \times (g - x_i^k)$$
(2)

$$x_i^{k+1} = x_i^k + v_i^{k+1} (3)$$

$$v_i^{k+1} = w \times v_i^k + c_1 \times r_1 \times (p_i - x_i^k) + c_2 \times r_2 \times (g - x_i^k)$$

$$x_i^{k+1} = x_i^k + v_i^{k+1}$$

$$w = -\frac{w_{min} - w_{max}}{k_{max}} \times k + w_{max}$$
(4)

Each particle generated by the PSO (i.e. each generated CRS geometry described with a set of parameters) is evaluated with the direct model. Simulation results are used to establish particles performance as they are the inputs of the target function f.

#### 3.1 A modified PSO

Furthermore, we implement the Guaranteed Convergence Particle Swarm Optimization algorithm (GCPSO) [15] in order to avoid early swarm convergence on the best position discovered so far. The global best position is then updated with another process to avoid stagnation phenomena. We assume that  $\tau$  is the index of this global best particle leading to:

$$g^k = p_{\tau}^k \tag{5}$$

To insure that the  $\tau$  particle keeps moving, a new velocity update equation is suggested in Eq. (6). The factor  $\rho$  permits to perform a random search around the best global position.  $\rho$  is a scaling factor defined after each time step as presented in Eq. (7).

$$v_{\tau}^{k+1} = -x_{\tau}^k + g^k + w \times v_{\tau}^k + \rho^k \times (1 - r_2) \tag{6}$$

$$\rho^{k+1} = \begin{cases} 2 \times \rho^k & \text{if } \#successes > s_c \\ 0.5 \times \rho^k & \text{if } \#failures > f_c \\ \rho^k & \text{otherwise} \end{cases}$$
 (7)

The terms #failures and #successes are the number of consecutive failures or successes whereas  $f_c$  and  $s_c$  are threshold parameters set with default value  $s_c = 5$  and  $f_c = 5$ . The test is a failure if  $f(g^k) = f(g^{k-1})$  and a success otherwise. The new position update for the  $\tau$  particle is presented in Eq.

$$x_{\tau}^{k+1} = g^k + w \times v_{\tau}^k + \rho^k \times (1 - r_2) \tag{8}$$

#### 4. NUMERICAL EXPERIMENTS

We use a C++ PSO library previously implemented. All computations are run on a Linux computer with AMD processors AMD Phenom II X6 1055T  $2.8 \mathrm{GHz}$  and  $12 \mathrm{Mo}$  RAM. Optimization tests are realized with 50 iterations for a swarm of 20 particles. The target function of each particle is evaluated with 5000 realizations of the Monte Carlo algorithm. With this amount of realizations, we insure a result with an uncertainty lower than 2%.

#### 4.1 Identification of the best parameters

To evaluate PSO performance, we introduce a test case. This case consists in a CRS where heliostats are composed of flat square mirrors as presented in the previous section. We take into account 3 parameters: the height of the tower, the size of mirrors and the number of mirrors by heliostat. The restriction on reflective area is set to  $15\,000\mathrm{m}^2$ . Table 1 presents parameters bounds and Table 2 presents PSO parameters and results for each test case. Under this circumstances, a complete optimization process is achieved in approximately  $1\mathrm{h}30\mathrm{min}$ .

Parameter	Lower bound	Upper Bound		
$H_t$	90m	110m		
$N_m$	1	81		
C	1m	2m		

Table 1. Parameters symbols, lower bound and upper bound

#### 4.2 Criteria of comparison

To make a comparison, we introduce some measurements of optimization methods performance. For each run, we calculate the normalized cost reduction defined in Eq.(9) and the distance to the maximum obtained reduction defined in Eq. (10).  $x^*$  is the particle with the highest target function for each test case,  $x^b$  is the reference case a with standard PSO parameters as presented by [14] and  $\hat{x}$  is the iterate with the highest target function value obtained by any of the tested optimization algorithm. We also want to check how particles converge towards the optimum. To do so, we introduce the mean and the relative standard deviation of the particles target functions.

$$r(x^*) = \frac{f(x^*) - f(x^b)}{f(x^b)}$$

$$(9)$$

$$d(r(x^*)) = r(\hat{x}) - r(x^*) = \frac{f(\hat{x}) - f(x^*)}{f(x^b)}$$
(10)

#### 4.3 Optimization performance

As presented in Tab. 2, it appears that results are very close regardless to parameters. In the meanwhile, the use of dynamic inertia leads to the appearance of a better target function optimum. The highest target function, achieved with the Ref. h (GCPSO,  $c_1=c_2=1.5$ ,  $w_{min}=0$ ,  $w_{max}=1.2$ ), is evaluated to 25.25GWh. The standard PSO (Ref. a) reaches the value of 25.22GWh and the Ref. b (PSO,  $c_1=c_2=0.5$ ,  $w_{min}=0$ ,  $w_{max}=1.2$ ) represents the more efficient PSO with a target function value of 25.24GWh. As observed with criteria of comparison, results are very close.

Table 2. Parameters of PSO algorithms, normalized cost reduction and distance to the maximum obtained cost reduction

Reference	Type of PSO	c <sub>1</sub> value	c <sub>2</sub> value	w <sub>min</sub> value	$w_{ m max}$ value	$\mathbf{r}(\mathbf{x}^*)$	$\mathbf{d}(\mathbf{r}(\mathbf{x}^*))$
a	PSO	2	2	1	1	0.00%	0.32%
b	PSO	0.5	0.5	0	1.2	0.31%	0.01%
c	PSO	1	1	0	1.2	-0.23%	0.55%
d	PSO	1.5	1.5	0	1.2	0.23%	0.09%
e	PSO	2	2	0	1.2	0.23%	0.09%
f	GCPSO	0.5	0.5	0	1.2	0.06%	0.26%
g	GCPSO	1	1	0	1.2	0.00%	0.32%
h	GCPSO	1.5	1.5	0	1.2	0.32%	0.00%
i	GCPSO	2	2	0	1.2	0.06%	0.09%

#### 4.4 Rate of convergence

To investigate swarm's convergence, we compare the standard PSO a with test cases b and h which obtain the highest target function value for respectively PSO and GCPSO algorithms. Fig. 2 represents swarm's mean for test cases a, b and h and Fig. 3 represents swarm's relative standard deviation for these 3 cases. We observe an erratic behavior for each case due to the non-smooth characteristic of the target function on both charts. However, the introduction of a dynamic inertia weight results in less irregular curve as observed for test cases b and b. Although best target functions values obtained with different PSO parameters are very close, as presented at section 4.3, the target function is highly unsmooth, making swarm convegence difficult to achieve.

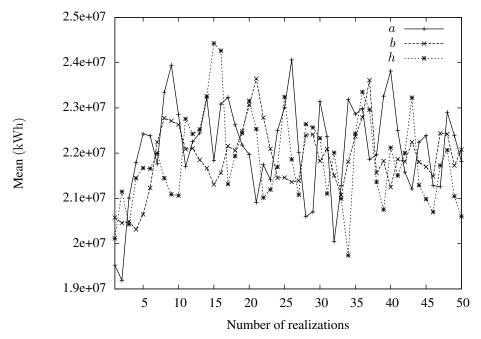


Fig. 2. Mean of swarm's target functions for test cases a, b and h

#### 4.5 PS10 redesign

As a validation case, we present a comparison between a model built using PS10 specifications (624 heliostats of  $120m^2$  and a 115m tower) and the result of an optimization run constrained by the PS10 land

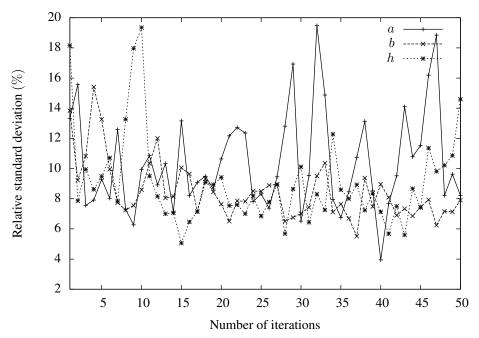


Fig. 3. Relative standard deviation of swarm's target functions for test cases a, b and h

surface area. The following conditions are set:

- Heliostats are made of flat mirrors with square facets;
- Heliostat field follows a radial staggered layout according to the MUEEN method;

Design parameters for optimization are the number of mirrors composing each heliostat and the width of each mirror. Doing so, the surface of mirrors can be significantly different. We compute this example with our tool. At the end of the process, the overall performance of the obtained CRS is increased by 14% compared to PS10 based CRS (annual thermal energy collected increasing from  $113.8 \mathrm{GWh}_{th}$  to  $130 \mathrm{GWh}_{th}$ ). This optimization routine is run during a reasonable computational time  $4\mathrm{h}$ .

#### 5. CONCLUSIONS AND FUTURE WORK

This paper introduced a new approach to design solar central receiver systems by coupling particle swarm optimizer and Monte Carlo method. The design tool developed is based on the maximization of the annual energy at the entrance of a solar receiver. This target function is highly non-smooth, making difficult to obtain a swarm convergence. A validation case is run using PS10 specifications to illustrate efficiency of the method presented. The redesign of this CRS leads to a significant improvement up to 14% of the annual thermal energy collected. In forthcoming work, the PSO algorithm will be hybridized with a Hookes-Jeeves algorithm in order to better accommodate the non-smooth characteristic. Moreover, the direct model will integrate the estimation of the electricity produced and the CRS plant investment cost so as to optimize the power production cost rather than the annual thermal energy collected. The Monte Carlo algorithm will be extended to estimate the production of a thermal cycle. We will also investigate the use of Kriging and metamodels in order to save computational time and increase the number of iterations and the size of swarms.

#### References

- 1. G. J. Kolb, S. A. Jones, M. W. Donnelly, D. Gorman, R. Thomas, R. Davenport, and R. Lumia, "Heliostat cost reduction study," tech. rep., 2007.
- 2. M. Sánchez and M. Romero, "Methodology for generation of heliostat field layout in central receiver systems based on yearly normalized energy surfaces," *Solar Energy*, vol. 80, no. 7, pp. 861 874, 2006.
- 3. X. Wei, Z. Lu, Z. Lin, H. Zhang, and Z. Ni, "Optimization procedure for design of heliostat field layout of a 1mwe solar tower thermal power plant," in *SPIE*, vol. 6841, p. 684119, 2007.
- 4. R. Pitz-Paal, N. B. Botero, and A. Steinfeld, "Heliostat field layout optimization for high-temperature solar thermochemical processing," *Solar Energy*, vol. 85, no. 2, pp. 334–343, 2011.
- 5. C. J. Noone, M. Torrilhon, and A. Mitsos, "Heliostat field optimization: A new computationally efficient model and biomimetic layout," *Solar Energy*, vol. 86, no. 2, pp. 792 803, 2012.
- 6. J. De La Torre, G. Baud, J. Bézian, S. Blanco, C. Caliot, J. Cornet, C. Coustet, J. Dauchet, M. El Hafi, V. Eymet, R. Fournier, J. Gautrais, O. Gourmel, D. Joseph, N. Meilhac, a. Pajot, M. Paulin, P. Perez, B. Piaud, M. Roger, J. Rolland, F. Veynandt, and S. Weitz, "Monte Carlo advances and concentrated solar applications," *Solar Energy*, May In Press, 2013.
- 7. E. J. Hoogenboom, "Zero-variance monte carlo schemes revisited," *Nuclear science and engineering*, vol. 160, no. 1, pp. 1–22, 2008.
- 8. A. De Lataillade, S. Blanco, Y. Clergent, J. Dufresne, M. El Hafi, and R. Fournier, "Monte carlo method and sensitivity estimations," *Journal of Quantitative Spectroscopy and Radiative Transfer*, vol. 75, no. 5, pp. 529–538, 2002.
- 9. M. Pharr and G. Humphreys, *Physically Based Rendering, second edition: from theory to implementation.* Morgan Kaufmann Publishers, 2010.
- 10. R. Osuna, V. Fernandez, M. Romero, and M. J. Marcos, "Ps10: A 10 mw solar thermal power plant for southern spain," in *Proceedings of 10th SolarPACES Conference*, (Sydney, Australia), July 2000.
- 11. F. M. F. Siala and M. E. Elayeb, "Mathematical formulation of a graphical method for a no-blocking heliostat field layout," *Renewable energy*, vol. 23, no. 1, pp. 77–92, 2001.
- 12. M. Roger, M. El Hafi, R. Fournier, S. Blanco, A. De Lataillade, V. Eymet, P. Perez, and É. d. M. d. Carmaux, "Applications of sensitivity estimations by monte carlo methods," in *The 4th International Symposium on Radiative Transfer*, 2004.
- 13. M. Wetter and J. Wright, "A comparison of deterministic and probabilistic optimization algorithms for nonsmooth simulation-based optimization," *Building and Environment*, vol. 39, no. 8, pp. 989–999, 2004.
- 14. J. Kennedy and R. Eberhart, "Particle swarm optimization," in *Neural Networks*, 1995. Proceedings., *IEEE International Conference on*, vol. 4, pp. 1942–1948, IEEE, 1995.
- 15. F. Van Den Bergh and A. P. Engelbrecht, "A new locally convergent particle swarm optimiser," in *Systems, Man and Cybernetics, 2002 IEEE International Conference on*, vol. 3, pp. 6–pp, IEEE, 2002.